Structure of an archaeal PCNA1-PCNA2-FEN1 complex: elucidating PCNA subunit and client enzyme specificity.

Article (Published Version)

Published online 31 August 2006 *Nucleic Acids Research, 2006, Vol. 34, No. 16* ***4515–4526***
doi:10.1093/nar/gkl623

Structure of an archaeal PCNA1–PCNA2–FEN1 complex: elucidating PCNA subunit and client enzyme specificity

Andrew S. Doré*, Mairi L. Kilkenny, Sarah A. Jones, Antony W. Oliver, S. Mark Roe, Stephen D. Bell[1] and Laurence H. Pearl*

CR-UK DNA Repair Enzymes Group, Section of Structural Biology, The Institute of Cancer Research, 237 Fulham Road, Chelsea, London, SW3 6JB, UK and [1]MRC Cancer Cell Unit, Hutchison MRC Research Centre, Hills Road, Cambridge, CB2 2XZ, UK

Received May 2, 2006; Revised and Accepted August 8, 2006

ABSTRACT

The archaeal/eukaryotic proliferating cell nuclear antigen (PCNA) toroidal clamp interacts with a host of DNA modifying enzymes, providing a stable anchorage and enhancing their respective processivities. Given the broad range of enzymes with which PCNA has been shown to interact, relatively little is known about the mode of assembly of functionally meaningful combinations of enzymes on the PCNA clamp. We have determined the X-ray crystal structure of the *Sulfolobus solfataricus* PCNA1–PCNA2 heterodimer, bound to a single copy of the flap endonuclease FEN1 at 2.9 Å resolution. We demonstrate the specificity of interaction of the PCNA subunits to form the PCNA1–PCNA2–PCNA3 heterotrimer, as well as providing a rationale for the specific interaction of the C-terminal PIP-box motif of FEN1 for the PCNA1 subunit. The structure explains the specificity of the individual archaeal PCNA subunits for selected repair enzyme 'clients', and provides insights into the co-ordinated assembly of sequential enzymatic steps in PCNA-scaffolded DNA repair cascades.

INTRODUCTION

DNA-binding processivity factors, such as the prokaryotic β-clamp and the archaeal/eukaryotic proliferating cell nuclear antigen (PCNA) provide stable anchorages on DNA for DNA modifying enzymes, whose functional mechanistic interaction with DNA is inherently transient (1). These toroidal structures are loaded onto DNA, encircling it to act as a sliding clamp and vastly increasing the processivity of attached enzymes (2).

In addition to replicative DNA polymerases, PCNA and its homologues have been shown to interact with a broad range of DNA modifying enzymes implicated in such DNA metabolic processes as DNA replication, Okazaki fragment maturation, DNA methylation, nucleotide excision repair (NER), mismatch repair (MMR) and long-patch base excision repair (LP-BER). In general, the principal interaction is mediated by recognition of a PCNA-interacting protein motif (PIP-box) of the 'client' enzyme, which binds the interdomain connector loop (IDCL) of a PCNA subunit (3). Examples of client DNA repair enzymes include: DNA glycosylases, such as MYH (4) NTH1 (5) and UNG (6); nucleases, such as FEN1 (7), APE1 (8) and APE2 (9), as well as DNA ligase I (10).

The multiple equivalent binding sites presented by an oligomeric toroidal clamp and the large number of possible PCNA clients that could be recruited, raises the question as to how assembly of functionally 'meaningful' combinations of clamp-bound enzymes is regulated. For example, a combination of PCNA-bound Pol δ, FEN1 and DNA Ligase 1 can restore a DNA strand following base excision by a glycosylase and AP-endonuclease, by extending the 3′ side of the gap, excising the displaced 5′-flap, and ligating the nick (7). However, a combination of PCNA-bound DNA glycosylases, UNG, MYH and NTH1, or PCNA loaded with three copies of FEN1 would be ineffectual. Furthermore, as reaction pathways of this type may potentially require a sequential 'hand-off' of intermediate products from one enzyme to the next (11), the correct order of enzymes around the ring also becomes important. Clearly some combinations may be precluded by steric clashes between large proteins (e.g. replicative polymerases), or favoured by evolved lateral contacts between enzymes bound to adjacent PCNA subunits.

*To whom correspondence should be addressed. Tel: +44 207 153 5453; Fax: +44 207 153 5457; Email: Andrew.Dore@icr.ac.uk
*Correspondence may also be addressed to Laurence H. Pearl. Tel: +44 207 153 5443; Fax: +44 207 153 5457; Email: Laurence.Pearl@icr.ac.uk
Present address:
Sarah A. Jones, Cancer Research UK, Genome Stability Laboratory, Clare Hall Laboratories, Blanche Lane, South Mimms, Herts, EN6 3LD, UK

However, structural studies of multiply loaded PCNA clamps have not provided supportive evidence for this so far (12).

In organisms, which utilize a homotrimeric PCNA system, the stoichiometry and composition of complexes with adaptor proteins is in principle stochastic. Thus, all possible productive and non-productive combinations of PCNA and adaptors may compete for access to a DNA lesion or growth point. However, the evolution of a heterotrimeric PCNA in *Sulfolobus solfataricus* suggests there is a selective pressure to favour meaningful combinations of adaptor/client proteins on the PCNA clamp and provides a useful system to investigate these specific adaptor protein interactions and molecular assemblies. The hyperthermophilic acidophile archaeon *S.solfataricus* contains three homologous but distinct PCNA genes, whose products form a heterotrimeric clamp with a defined composition and order of assembly. PCNA1 and PCNA2 form a stable heterodimer, the generation of which is a prerequisite for binding PCNA3 (13). Each subunit in the active *S.solfataricus* PCNA heterotrimer displays preferential binding to a subset of client enzymes. Thus, the archaeal FEN1 binds PCNA1, DNA Polymerase B1 binds PCNA2, DNA Ligase 1 and UDG bind PCNA3, while XPF binds PCNA1 and PCNA3 (13–15).

Here we report the 2.9 Å crystal structure of the *S.solfataricus* PCNA1–PCNA2 heterodimer in complex with FEN1. The PCNA1-2 heterodimer structure demonstrates specificity and chirality for its own toroidal ring assembly as demonstrated by the co-crystal structure, modelling of the PCNA heterotrimer and mutational data. In addition, the PCNA subunits demonstrate specificity for the client proteins to which they bind through structural differences between their inter-domain connecting-linker (IDCL) segments.

MATERIALS AND METHODS

Protein expression and purification

Recombinant plasmid DNA coding for *S.solfataricus* PCNA1, PCNA2, PCNA3 and FEN1 were subcloned into pET11a (Novagen), pGEX-6P1 (GE Healthcare), pET30a (Novagen) and pET33b (Novagen), respectively. All three proteins were expressed separately in the *Escherichia coli* ROSETTA™ (Novagen) BL21 (DE3) host strain for 20 h at 293 K with addition of 1 mM isopropyl-β-D-thiogalactoside (IPTG).

PCNA1, PCNA2 and PCNA3 cell pellets were combined and resuspended in buffer containing 20 mM Tris–HCl (pH 7.5), 200 mM NaCl, 1 mM DTT supplemented with complete EDTA-free protease inhibitors (Roche). The cells were disrupted by sonication and the bacterial lysate clarified by centrifugation at 48 384 *g* for 60 min using a Beckman JA-20 rotar. Soluble cell lysate was then applied to Glutathione Sepharose 4B (GST) resin (GE Healthcare) and extensively washed in 20 mM Tris–HCl (pH 7.5), 200 mM NaCl and 1 mM DTT. The Glutathione Sepharose 4B resin was then resuspended in 20 mM Tris–HCl, 50 mM NaCl and 1 mM DTT, and incubated with PreScission Protease for 20 h at 277 K to remove the GST tag from PCNA2. The PCNA1–PCNA2 complex was then washed off the GST resin and applied to a Hi-Trap QHP (GE Healthcare) anion exchange column. The PCNA1–PCNA2–PCNA3 complex was eluted, and purified to homogeneity, with a linear gradient from 50 to 800 mM NaCl in buffer containing 20 mM Tris–HCl (pH 8.0) and 1 mM DTT.

FEN1 cell pellets were resuspended in buffer containing 50 mM (N-morhpolino)ethanesulfonic acid (MES) (pH 6.5), 50 mM NaCl, 5 mM $MgCl_2$, 1 mM DTT supplemented with Complete EDTA-free protease inhibitors. The cells were disrupted by sonication and the bacterial lysate clarified by centrifugation at 48 384 *g* for 60 min using a Beckman JA-20 rotar. Soluble cell lysate was subsequently incubated at 343 K for 15 min, followed by incubation at 277 K for 10 min to thermoprecipitate host proteins. Precipitated protein was then removed by centrifugation at 48 384 *g* for 60 min using a Beckman JA-20 rotar. Clarified soluble lysate containing FEN1 from the thermoprecipitation step was then applied to a Hi-Trap SP (GE Healthcare) cation exchange column and FEN1 eluted in a linear gradient from 50 to 900 mM NaCl. Fractions containing recombinant FEN1 were then dialysed against buffer containing 50 mM MES (pH 6.5), 30 mM NaCl, 5 mM $MgCl_2$, 1 mM DTT, applied to a Hi-Trap Heparin HP column (GE Healthcare) and eluted in a linear gradient from 30 to 700 mM NaCl. Finally, a size exclusion chromatographic step using a 16/60 Superdex S200 column (GE Healthcare) was employed to purify FEN1 to homogeneity.

Crystallization

Prior to crystallization the PCNA1–PCNA2–PCNA3 complex was mixed with FEN1 at an equimolar ratio and incubated for 20 min at 294 K. PCNA1–PCNA2–FEN1 co-crystals were grown by the vapour diffusion method in hanging drops (space group $P2_12_12_1$ a = 93.99 Å, b = 99.77 Å, c = 99.96 Å) with one copy of the PCNA1–PCNA2 heterodimer and one copy of FEN1 per asymmetric unit. PCNA3 was not present in the crystal lattice presumably as a consequence of the lower binding affinity of this subunit compared with the PCNA1–PCNA2 heterodimer (13). Drops were prepared by mixing 100 μM protein complex in 20 mM Tris–HCl (pH 8.0), 200 mM NaCl, 5 mM $MgCl_2$, 2 mM DTT buffer solution with equal volumes of 0.1 M Acetate (pH 4.8), 8% PEG 8000, 220 mM $ZnOAc_2$ and 30 mM glycyl–glycyl–glycine. Crystals appeared after 48 h, and took two weeks to reach maximum dimensions of 400 × 300 × 400 μm.

Data collection, model building and refinement

Diffraction data from cryo-cooled native crystals was collected at ID23-1 of the European Synchrotron Radiation Facility (ESRF) in Grenoble, France at a wavelength of 0.9795 Å. Images were integrated and scaled using the programs MOSFLM (16) and SCALA (17). The number of observed reflections corresponds to a 99.2% complete dataset to 2.9 Å resolution. Molecular replacement was performed using the PHASER program (18) initially searching for one copy of FEN1 from *Pyrococcus furiosus* (19) (PDB code:1B43) and subsequently for two copies of a human PCNA monomer (20) (PDB code: 1VYJ). Extensive crystallographic modelling was performed using the program COOT (21), and crystallographic refinement performed using simulated annealing in the CNS package (22) and TLS/restrained

Table 1. Data collection and refinement statistics (molecular replacement)

	PCNA1–PCNA2–FEN1
Data collection	
Space group	$P2_12_12_1$
Cell dimensions	
a, *b*, *c* (Å)	93.99, 99.77, 99.96
Resolution (Å)	30–2.90 (2.975–2.90)[a]
R_{merge}	0.082 (0.443)
$I/\sigma I$	6.9 (1.6)
Completeness (%)	99.2 (99.8)
Redundancy	4.8 (4.9)
Refinement	
Resolution (Å)	30–2.90
No. reflections	20 108
R_{work}/R_{free}	0.251/0.310
No. atoms	
Protein	5708
Ligand/ion	4 Zn^{2+}/3 Mg^{2+}
Water	81
B-factors	
Protein	59.7
Ligand/ion	62.7
Water	40.5
R.m.s deviations	
Bond lengths (Å)	0.007
Bond angles (°γ°)	1.026

All diffraction data were collected from one crystal.
[a]Highest resolution shell data are shown in parentheses

refinement using the REFMAC 5 package (23). The refined model comprises 5708 protein atoms and 81 water molecules (Table 1). Of the 753 amino acid residues, 98.4% are in the allowed region of the Ramachandran plot, 1.4% in the generously allowed region and 0.2% in the disallowed region. Five regions of FEN1 are disordered in the electron density map. All figures were prepared using PyMOL (24).

Determination of PCNA heterotrimer chirality by mutagenesis of the inter-subunit interfaces of *S.solfataricus*

Mutations were introduced into the N-terminal (114-YIK-116 to 114-ELE-116) and C-terminal (175-KRY-177 to 175-EED-177) inter-subunit interfaces of *Sso*–PCNA1 and the C-terminal interface of *Sso*–PCNA2 (E146K, D149K) using oligonucleotide-mediated site directed mutagenesis. The mutations were introduced into the pGex4T3–PCNA1 or pGex4T3–PCNA2 construct and recombinant protein purified as described previously (13). GST pull downs were performed as described previously (13).

RESULTS

Architecture *of the S.solfataricus* PCNA1–PCNA2–FEN1 complex

The PCNA1–PCNA2–FEN1 complex consists of a single copy of *Sso*–FEN1 (346 amino acids) bound to *Sso*–PCNA1 (249 amino acids), which itself forms a heterodimer with *Sso*–PCNA2 (246 amino acids)—see Table 1 for crystallographic statistics. *Sso*–FEN1 binds via its C-terminus, to the IDCL segment of *Sso*–PCNA1, and is orientated, such that the axis of the DNA-binding groove of *Sso*–FEN1 (11) is perpendicular to the plane of the *Sso*–PCNA1–PCNA2 heterodimer partial toroidal ring (Figure 1).

Structure of *S.solfataricus* FEN1

The structure of the nuclease core domain of *S.solfataricus* FEN1 (residues 1–331) closely resembles previously determined FEN1 structures, consisting of a central six-stranded β-sheet flanked by α-helices, creating a central groove, which accommodates the active site residues important for DNA-binding and phosphodiester backbone cleavage (12,25).

The structure of FEN1 from the archaeon *Archaeoglobus fulgidus*, bound to a dsDNA substrate with a single nucleotide 3′ flap, has recently been determined (11). *Afu*–FEN1-bound to this DNA, which is believed to represent a repair intermediate, shows a number of conformational differences from the apo form of the enzyme. Specifically, the α-4–α-5 region of *Afu*-FEN1 becomes ordered to create a helical clamp and the α-2–α-3 loop undergoes a ∼5 Å shift to create a 'hydrophobic wedge', which packs against the terminal base pair of the DNA (11). In the PCNA1-bound *Sso*–FEN1 structure, the α-4–α-5 region is mostly disordered and the α-2–α-3 loop is in a conformation expected for the apo form of FEN1. However, other residues in *Sso*–FEN1 involved in 3′ flap substrate recognition superpose well with the *Afu*–FEN1–DNA structure.

Structure of the *S.solfataricus* PCNA1–PCNA2 heterodimer

Sso–PCNA1 and PCNA2 heterodimerize to form two-thirds of the classical eukaryotic trimeric PCNA toroidal ring, and represent the first structure of a PCNA dimer determined to date. Both *Sso*–PCNA subunits are composed of two topologically identical N- and C-terminal domains, with each domain itself consisting of two β−α−β−β−β motifs. In the *Sso*–PCNA1–PCNA2 heterodimer, three β-sheets form the outer surface of the partial ring and support eight α-helices lining the inside. The N- and C-terminal domains in each PCNA subunit are then connected by the IDCL, which lies on the 'outer' surface of the partial ring.

The overall architecture and arrangement of secondary structure elements observed in eukaryote PCNAs, are conserved in the *Sso*–PCNA heterodimer; superposition of the separate human PCNA N- and C-terminal domains (PDB code: 1VYJ) (20) onto their equivalents in *Sso*–PCNA1 and PCNA2 gives r.m.s.d. deviations of 1.89 Å/1.21 Å and 1.06 Å/1.28 Å, respectively across 90 equivalent Cα atoms. However, within this overall structural similarity, the inter-domain connecting-linker segments that provide the binding site for PCNA client proteins differ considerably between the eukaryotic PCNA monomer, and the *Sso*–PCNA1 and PCNA2 subunits (see below).

Whilst the *Sso*–PCNA2 N- and C-terminal domains are related by the pseudo 2-fold symmetry also observed in eukaryote PCNA, the N-terminal domain of PCNA1 is rotated by ∼3° about an axis perpendicular to the plane of the partial ring. While we cannot dismiss the possibility that this is a result of crystal packing interactions, this additional twist between the domains of *Sso*–PCNA1 may be induced by heterodimerization with *Sso*–PCNA2 and may

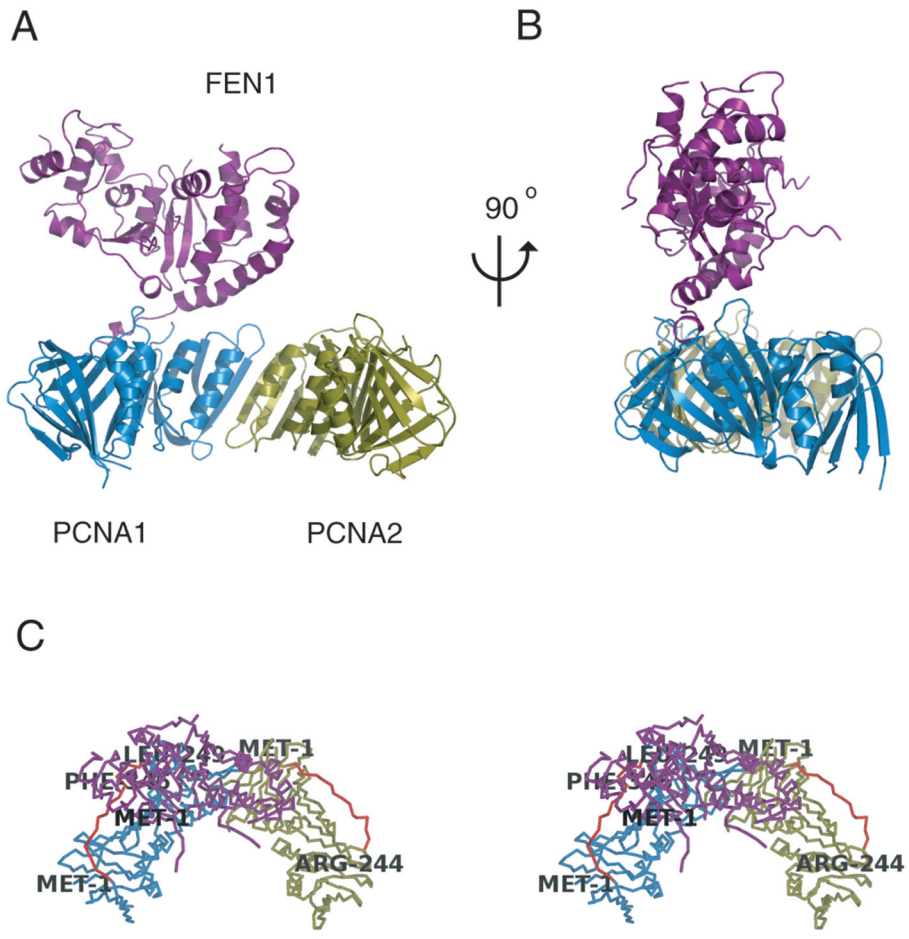

Figure 1. (**A**) The crystal structure of the *Sso*–PCNA1:PCNA2:FEN1 complex, determined to 2.9 Å resolution. (**B**) Structure as shown in (A), rotated by 90° about axis as shown. PCNA1, PCNA2 and FEN1 are shown in cartoon representation, coloured blue, olive and purple, respectively. (**C**) Cα stereo trace of the PCNA1–PCNA2–FEN1 complex structure, coloured as in (**A** and **B**). The inter-domain connecting linkers of the PCNA subunits are shown in red. The N- and C-terminal residues of each protein are labelled.

be a prerequisite for binding *Sso*–PCNA3, which only occurs after assembly of a PCNA1–PCNA2 heterodimer (13).

The PCNA1–FEN1 interface

In all structures determined to date involving PCNA or related clamps, and an interacting client replication or repair protein, or more commonly a peptide derived thereof, the interacting segment of the client protein typically adopts a 3_{10}-helical turn and inserts two hydrophobic/aromatic residues into pockets formed by the outer surface of the eight-stranded beta sheet and IDCL of the PCNA subunit. These interactions are furnished by the residues forming the consensus PIP-box - Qxx(M/L/I)xxF(Y/F) (26), which serves to anchor the client protein to the clamp. The client polypeptide N-terminal of the PIP-box typically makes a short antiparallel β-zipper interaction with the C-terminal strand of the clamp subunit, while the client sequence C-terminal of the 3_{10}-helical turn forms an extended beta sheet with the IDCL (3,27–29).

While the interaction of *Sso*–FEN1 with *Sso*–PCNA1 resembles that of the peptide derived from *A.fulgidus* FEN1-bound to *Afu*–PCNA (11), and the human FEN1–PCNA complex (12), there are distinct differences. Unlike the human FEN1–PCNA interaction, the PIP-box motif from *Sso*–FEN1 is provided by the extreme C-terminal sequence (339—QTGLDRWF-COOH—346), and thus does not form an extended β-sheet with the IDCL. However, in an analogous mechanism to the classical PIP-box interaction motif as seen in the peptide derived from *A.fulgidus* FEN1-bound to *Afu*–PCNA, Phe346 and Trp345 make a double hydrophobic ball-and-socket joint with PCNA1 (Figure 2A). Residues Leu40, Met47, Thr126, Pro128 of PCNA1 and Leu342 of the PIP-box motif in FEN1 provide the hydrophobic pocket for Phe346. The hydrophobic pocket for Trp345 is provided by Pro128, Val130, Leu227, Pro228, Pro247 of PCNA1 and Thr340, Leu342 of FEN1 and capped by the aliphatic portion of the Arg344 side chain of FEN1.

The highly conserved Gln339 from the *Sso*–FEN1 PIP-box performs an analogous role to the glutamine in the *Afu*-FEN1 PIP-box derived peptide:PCNA complex (PDB code: 1RXZ) (11) and makes a water-mediated hydrogen bond to the main-chain carbonyl of Ala246 in PCNA1. In addition, *Sso*–FEN1 Gln339 also makes a hydrogen bond to Arg248 of PCNA1. The intervening residue between Ala246 and Arg248 is a proline and conserved across the PCNA orthologs. Indeed,

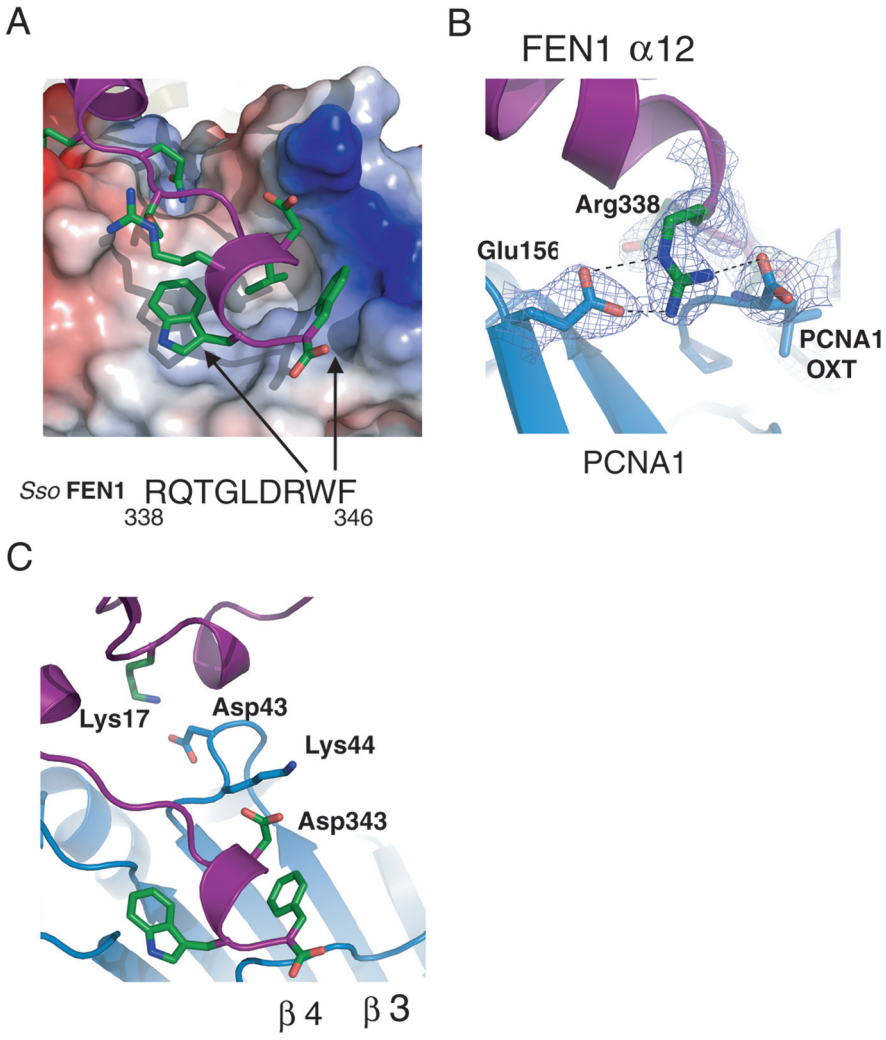

Figure 2. (**A**) Interaction between the C-terminal PIP-box of *Sso*–FEN1 (purple) and PCNA1 (shown as electrostatic potential surface). Arrows indicate the hydrophobic double ball-and-socket joint comprising the terminal Trp345 and Phe346 residues of FEN1. (**B**) Interaction and hydrogen-bonding network formation between Arg338 situated on the C-terminus of the α12 helix of *Sso*–FEN1 with Glu156 and the C-terminal oxygen of PCNA1, $2F_o - F_c$ electron density is contoured at 1.5 σ. The formation of this 'polar-cap' on the β-zipper maintains its trajectory and the resultant position of FEN1 on the PCNA1-2 heterodimer. (**C**) An additional protein–protein interface involving residues in the β-3–β-4 intervening loop of PCNA1 with both the PIP-box motif and the N-terminal region of *Sso*–FEN1 contributes to the resultant conformation of *Sso*–FEN1 on the PCNA1-2 heterodimer. The side-chains of Asp43 and Lys44 from PCNA1 form salt bridges with Lys17 and Asp343 of FEN1, respectively.

this proline has previously been proposed to act as a rigid joint at the base of the β-zipper (formed by residues Gln339–Thr340 of FEN1 and Pro247–Arg248 of PCNA1), which directs it away from the PCNA surface and prevents spurious interactions with other PCNA residues (11). Through hydrogen-bonding to residues on either side of Pro247 the trajectory of the β-zipper is highly dependent upon Gln339 in FEN1 and also upon the restricted peptide conformation backbone of Pro247 itself. However, a number of other residues play an important role in directing the trajectory of the β-zipper in the *Sso*–PCNA1–PCNA2–FEN1 structure.

The C-terminal helix (α-12) of *Sso*–FEN1 makes an extra turn before the β-zipper in comparison to the human PCNA–FEN1 structure (PDB code: 1UL1, chain Y). Arg338 of *Sso*–FEN1 is situated on this extra turn of the α-12 helix and forms a hydrogen-bonding network with Glu156 and the C-terminal oxygen of PCNA1 (Figure 2B). Glu156 is then poised to form a hydrogen bond with Arg248 of PCNA1 and contributes towards maintaining the conformation of the zipper. Thus, the formation of this 'polar-cap' on the β-zipper maintains its trajectory and the resultant position of FEN1 on the PCNA1-2 heterodimer. This additional interaction between the C-terminus of PCNA1 and FEN1 in comparison to the human PCNA–FEN1 structure may be required to compensate for the C-terminal truncation of *Sso*–FEN1, which results in loss of the intermolecular β-sheet with the IDCL of the PCNA subunit (12).

In addition, interaction of residues in the β-3–β-4-intervening loop of PCNA1 (residues Asp43 and Lys44) with both the PIP-box motif and the N-terminal region of FEN1 complete the *Sso*–PCNA1–FEN1 interface. The side-chains of Asp43 and Lys44 from PCNA1 form salt bridges with Lys17 and Asp343 of FEN1, respectively (Figure 2C).

Finally, Lys44 makes a main-chain hydrogen bond to Leu342 in the PIP-box motif of FEN1.

The PCNA1–PCNA2 heterodimer interface

Antiparallel interactions between the strands in adjacent PCNA subunits are the key elements in the intermolecular PCNA interface and contribute to the formation of three β-sheets that form a contiguous surface across each intermolecular boundary in the ring. In the *Sso*–PCNA1–PCNA2 interface these intermolecular β-sheets involve β-13 of PCNA1 and β-9 of PCNA2. However, further interactions are made between the side-chains of residues participating in the intermolecular sheet and involve α-3 and α-2 of PCNA1 and PCNA2 situated on the inside of the ring at the heterodimer interface. These interactions are responsible for the specificity of the PCNA subunit interactions, and hence for the specific chirality of subunit order in the assembly of the *Sso*–PCNA heterotrimer.

The β-13, β-9, α-3, α-2 interface produces alternating buried polar and hydrophobic patches, which determine the *Sso*–PCNA subunit specificity. An exceptional feature of the *Sso*–PCNA1–PCNA2 interface is the central buried polar interactions that are mediated by Arg82 and Arg108 on α-2 and β-9 of PCNA2, respectively (Figure 3A). Arg82 makes a hydrogen bond to the main-chain carbonyl of Val145 of PCNA1 while also making a salt bridge with Asp149 of PCNA1. Asp149 of PCNA1 then makes a hydrogen bond to Tyr177 of PCNA1, thus becoming poised to make an additional hydrogen bond with Arg108 of PCNA2. The side chain of Arg108 of PCNA2 is itself held in place to participate in this interaction with Asp149 through a bifurcated hydrogen bond to the main-chain carbonyl of Arg82 of PCNA2. Finally Asp87 of PCNA2 fully satisfies the hydrogen-bonding potential of Arg108 through a salt bridge and water-mediated hydrogen bond (Figure 3A).

Extensive hydrophobic interfaces flank the central polar interactions of PCNA1–PCNA2. On the opposite side of the PCNA ring to the IDCL these are formed by Leu84, Phe106, the aliphatic portion of the Arg108 side chain from PCNA2 and Val142, Val145, Ile146 and Leu181 from PCNA1. On the other side Ile79, Phe110, the aliphatic portion of the Arg82 side chain of PCNA2 and Val150, Leu152 and Val153 of PCNA1 form this hydrophobic interface. Finally, Lys175 at the N-terminal end of β-13 from PCNA1 hydrogen bonds to Asp75 from the N-terminal end of α-2 from PCNA2 and completes the polar-hydrophobic stripes across the heterodimeric interface (Figure 3B).

Mutational analysis of *S.solfataricus* PCNA subunit interfaces

PCNA has distinct front and back faces, with subunits interacting in a head-to-tail manner. Therefore, the heterotrimeric ring of *S.solfataricus* PCNA could adopt one of two conformations PCNA1–PCNA2–PCNA3 or PCNA2–PCNA1–PCNA3. To determine the polarity of the subunits in solution, and to corroborate the structural data presented here, point mutations were introduced into the *Sso*–PCNA1 and *Sso*–PCNA2 open reading frame in either the N- or C-terminal inter-subunit interaction β-strands (β-9 and β-13, respectively). Wild-type and the N- and C-terminally mutated derivatives (P1N and P1C) of PCNA1, and wild-type and a C-terminally mutated version of PCNA2 (P2C) were then made as GST fusion proteins and used in pull-down assays with the other subunits.

As can be seen in Figure 4, lane 7, and mutation of the *Sso*–PCNA1 N-terminal strand of the sequence 114-Tyr-Ile-Lys-116 to 114-Glu-Leu-Glu-116 (resulting in predicted charge repulsion to E169 of *Sso*–PCNA3) abrogated interaction with *Sso*–PCNA3 but left *Sso*–PCNA2 binding essentially unaltered. Additionally, we mutated the C-terminal–PCNA3

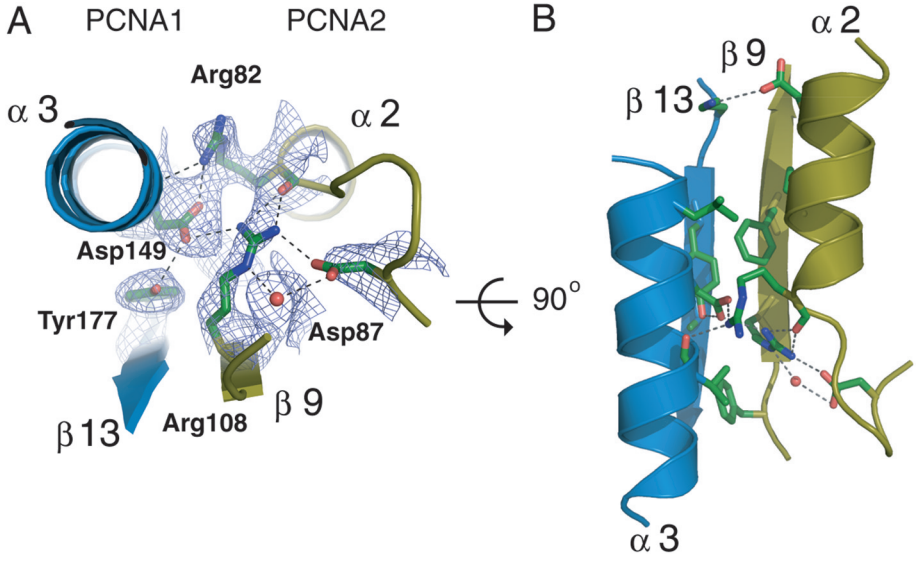

Figure 3. (**A**) The interface between *Sso*–PCNA1 and PCNA2. OMIT map electron density is contoured at 1.0 σ around residues involved in the buried charged hydrogen-bonding network at the subunit interface. PCNA1 and PCNA2 are coloured blue and olive, respectively. (**B**) View as in (A), rotated by 90° about axis as shown. Electron density has been removed for clarity. In this orientation the hydrophobic residues surrounding the central charged hydrogen-bonding network are clearly visible.

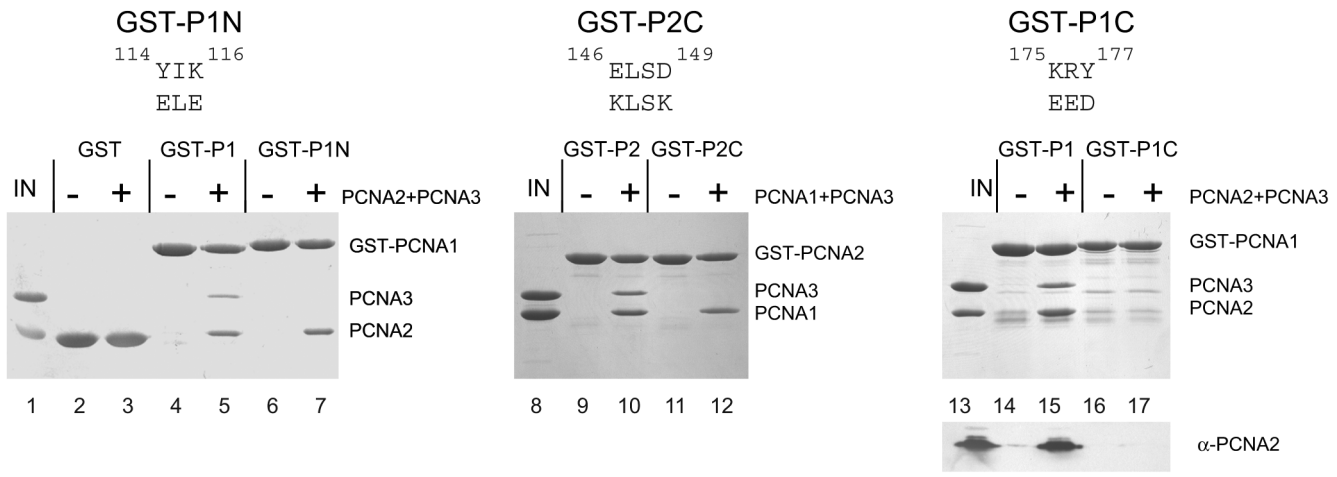

Figure 4. Coomassie-stained gels demonstrating the polarity of *S.solfataricus* PCNA in solution. GST pull downs were performed with 10 μg of GST (lanes 2 and 3), GST-PCNA1 (lanes 4, 5, 14 and 15), GST–PCNA2 (lanes 9 and 10), GST–PCNA1 N-terminal interaction site mutant (lanes 6 and 7, GST-P1N), GST–PCNA2 C-terminal interaction site mutant (lanes 11 and 12, GST-P2C) or GST–PCNA1-C-terminal interaction site mutant (lanes 16 and 17, GST-P1C) fusion proteins in the presence (+) or absence (−) of 10 μg of *Sso*–PCNA1 and *Sso*–PCNA3 or *Sso*–PCNA2 and *Sso*–PCNA3 as indicated. Lanes 1 and 13 contain 5 μg each of *Sso*–PCNA2 and *Sso*–PCNA3, lane 8 has 5 μg each of *Sso*–PCNA1 and *Sso*–PCNA3. Because *Sso*–PCNA2 co-migrates with a breakdown product of GST-P1 and GST-P1C present in lanes 14–17, the samples were subjected to western blotting using anti- *Sso*–PCNA2 antisera; the result is shown in the lower panel.

interaction—interface of PCNA2 by making the changes Glu146Lys and Asp149Lys. These mutations abolished *Sso*–PCNA3 interaction but left *Sso*–PCNA2's interaction with *Sso*–PCNA1 unaltered (compare Figure 4, lanes 10 and 12). Thus, these observations are fully consistent with an arrangement for the heterotrimer in which *Sso*–PCNA3 interacts with the N-terminal interaction strand of *Sso*–PCNA1 and the C-terminal interaction strand of *Sso*–PCNA2. Further, mutation of *Sso*–PCNA1's C-terminal interaction strand of the sequence K175-Lys-Arg-Tyr-177 to 175-Glu-Glu-Asp-177 resulted in loss of both *Sso*–PCNA2 and *Sso*–PCNA3 binding (see Figure 4, lane 17). Taken together, these data reveal the importance of electrostatic interactions in defining inter-subunit interactions, support the polarity of the *Sso*–PCNA ring indicated by the crystal structure and confirm that formation of the *Sso*–PCNA1–PCNA2 heterodimer is an essential prerequisite for recruitment of PCNA3.

DISCUSSION

Specificity of *S.solfataricus* PCNA heterotrimer assembly

The crystal structure of the isolated PCNA3 subunit from the related archaeon *Sulfolobus tokodaii*, which has 62% identity to *Sso*–PCNA3, has recently been determined (PDB code: 1UD9). Sequence threading of the *S.solfataricus* PCNA3 sequence onto 1UD9 and subsequent superposition of the N-terminal and C-terminal domains onto the human PCNA monomer (from 1UL1.pdb) results in an N- and C-domain root mean square deviation (r.m.s.d.) of 1.30 Å/1.14 Å, respectively across 90 equivalent secondary structure Cα positions. Thus, a good working model for the full *Sso*–PCNA heterotrimer can be constructed.

The structure of the *S.solfataricus* PCNA1–PCNA2 heterodimer, and the *Sso*–PCNA1–PCNA2–PCNA3 heterotrimer model presented here provide a unique insight into the molecular specificity of the PCNA heterotrimer assembly. This specificity is dependent on both surface electrostatic 'lock-and-key' complementarity at subunit interfaces and the pattern of hydrogen-bonding residues presented in the mainly hydrophobic subunit interface.

Structures of other PCNA and β-clamp rings show a conserved subunit interface structure, involving formation of an intermolecular β-sheet and a helix–helix interaction. In the bacterial β-clamp, the N- and C-terminal regions of each of the two subunits display marked charge asymmetry, with the N-terminal interface being mainly positive and the C-terminal interface mainly negatively charged (30). Four hydrogen bonds constitute the intermolecular β-sheet and six ion pairs from residues at the interface surround a small hydrophobic core. The resultant electrostatic asymmetry leads to a head-to-tail assembly of the homodimer (29,30). In human PCNA (31), the intermolecular β-sheet involves eight hydrogen bonds, but only one ion-pair between different subunits, in an otherwise predominantly hydrophobic interface.

The *Sso*–PCNA heterotrimer assembly reflects aspects of both the homotrimeric eukaryotic PCNA, and homodimeric bacterial β-clamp interfaces; the intermolecular β-sheet between *Sso*–PCNA1 and *Sso*–PCNA2 involves five main-chain hydrogen bonds and three ion pairs—Asp75, Arg82 and Arg108 of *Sso*–PCNA2, and Asp149 and Lys175 of *Sso*–PCNA1. Inspection of the electrostatic surface potential of each of these subunit interfaces reveals a striking pattern of charge complementarity surrounding a 'C-shaped' hydrophobic core (Figure 5). Furthermore, mutation of both Lys175 and Arg176 of PCNA1 to glutamate resulting in charge repulsion disrupts the *Sso*–PCNA1–PCNA2 interface. This demonstrates the strong dependence of subunit interactions on these complementary electrostatics.

Comparisons of the electrostatic surface potential of the *Sso*–PCNA1 N-terminal domain and the *Sso*–PCNA2 C-terminal domain with the subunit interfaces of the

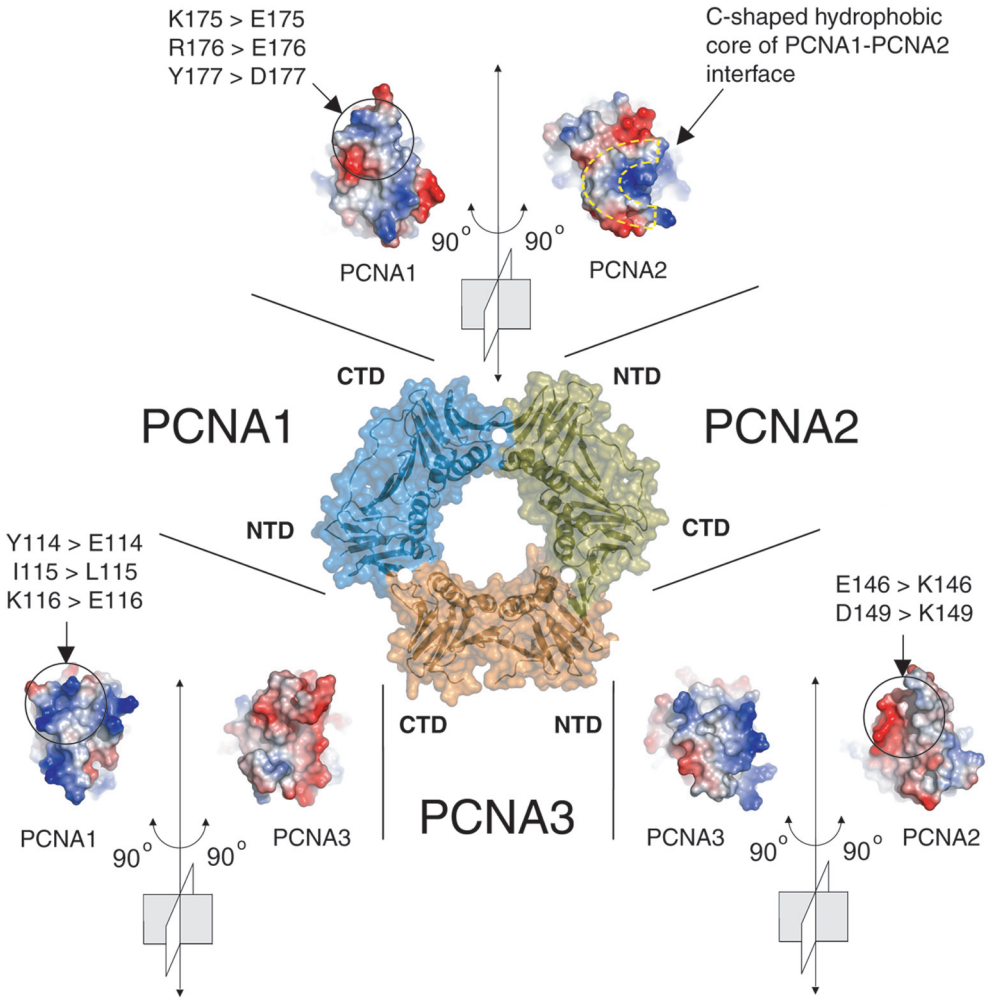

Figure 5. Electrostatic potential surface representations of the interface between the *Sso*–PCNA1–PCNA2–PCNA3 heterotrimer. NTD and CTD indicate N-terminal and C-terminal domains, respectively. It should be noted that PCNA3 has been modelled to generate the heterotrimeric PCNA ring. Axes perpendicular to the plane of the PCNA ring and at the interface between subunits are marked with a white circle. Each PCNA interface has been opened and rotated by 90° around the axes marked on the heterotrimer to demonstrate the 'lock-and-key' electrostatic complementarity between adjacent subunits. Residues participating in the electrostatic interface that have been mutated are indicated by '>'. The C-shaped hydrophobic interface flanked by charged patches on the PCNA1–PCNA2 interface is labelled.

Sso–PCNA3 model, show complementary electrostatic patterns, which are non-interchangeable (Figure 5). This electrostatic 'lock-and-key' model, which obviates homomeric interactions by the *Sso*–PCNA1, *Sso*–PCNA2 and *Sso*–PCNA3 subunits, and mediates a unique and heterotrimeric arrangement, is supported by the effect of the Lys116Glu mutation in *Sso*–PCNA1. This mutation is predicted to disrupt an ion-pair with Glu169 of *Sso*–PCNA3 and abrogates the interaction of *Sso*–PCNA1 with *Sso*–PCNA3.

S.solfataricus PCNA—client protein specificity

Comparison of human PCNA structures in the presence or absence of bound client protein/peptide demonstrate little change in the main-chain conformation of the IDCL as a result of binding to the PIP-box motif (3,12), suggesting that there is relatively little induced-fit accompanying client binding. The structural basis for the selective recruitment of *Sso*–FEN1 to *Sso*–PCNA1 but not the other subunits can thus be understood by comparison of the binding sites in terms of the interactions they offer to the specific PIP-box motif of *Sso*–FEN1.

When prospective binding of *Sso*–FEN1 to *Sso*–PCNA2 is modelled by superimposition of *Sso*–FEN1–PCNA1 onto *Sso*–PCNA2, it is immediately clear that the insertion of Phe346 into a hydrophobic pocket in *Sso*–PCNA2, as observed in the interaction with *Sso*–PCNA1, is sterically precluded by a direct clash with Pro123 in the sequence 121-Gln-Pro-Pro-Ser-124 in the *Sso*–PCNA2 IDCL (Figure 6C). The rigid stereochemical constraints imposed across this region by the double proline, provide the main determinant for precluding binding (or a conformational change to accommodate) Phe346 from *Sso*–FEN1. Furthermore Glu156, which participates in the 'polar-cap' of the β-zipper formed between the PIP-box of *Sso*–FEN1 and *Sso*–PCNA1, is replaced by a valine in PCNA2, adding to the disfavouring of *Sso*–FEN1 binding. Finally, the IDCL of PCNA1 adopts a unique conformation in comparison to all other known

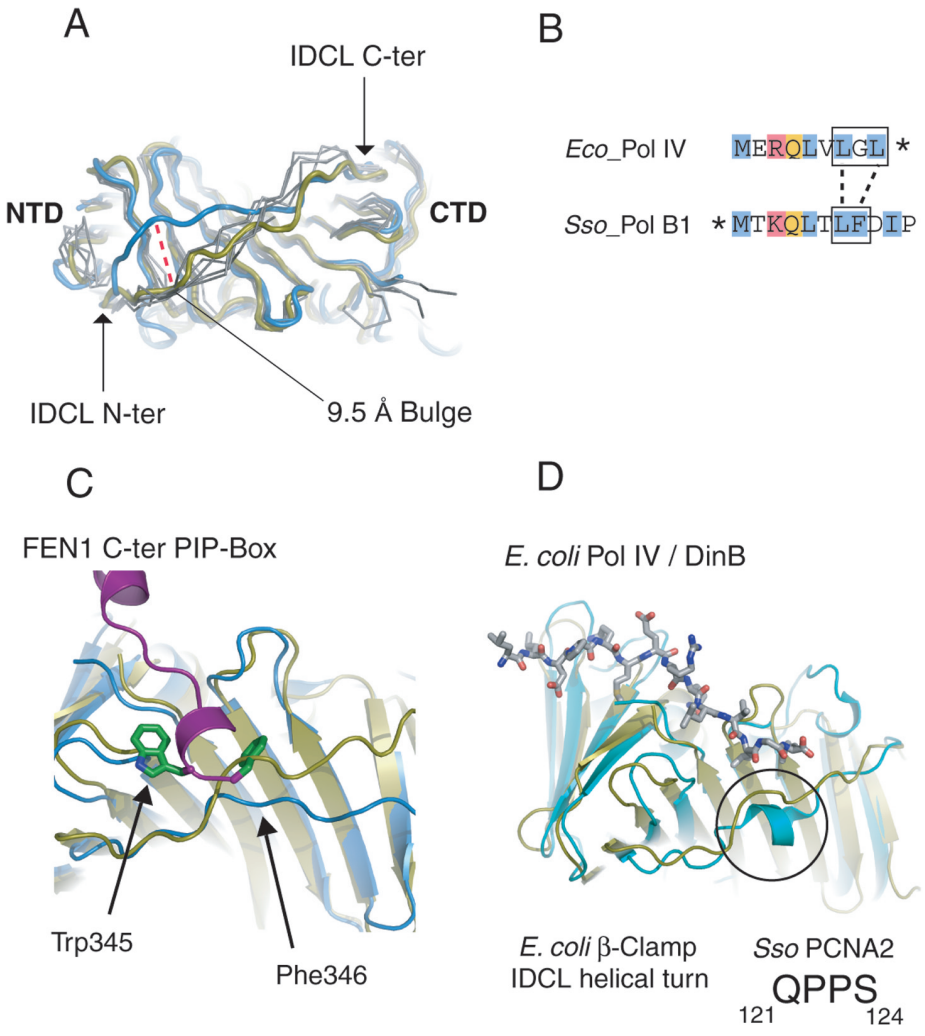

Figure 6. (**A**) Structural superposition of *Sso*–PCNA1 (blue) and *Sso*–PCNA2 (olive) with human PCNA (PDB codes: 1UL1, 1U76, 1VYM), *Saccharomyces cerevisiae* PCNA (pdb code: 1PLR) and the model of *Sso*–PCNA3 (shown in grey). (**B**) Sequence alignment of observed and postulated PCNA-interacting motifs from *E.coli* Polymerase IV and *Sso*-DNA Polymerase B1. The conserved glutamine is coloured orange. Residues marked in blue and red denote important clamp-interacting hydrophobic and polar residues, respectively. The structurally equivalent -LeuPhe-/-Leu-Gly-Leu motifs are highlighted by a black box. N- and C-termini of protein sequences are denoted by *. (**C**) Structural superposition of *Sso*–PCNA2 (olive) onto *Sso*–PCNA1 (blue). The FEN1 C-terminal PIP-box residues are shown in cartoon representation coloured purple, with the side-chains of residues Trp345 and Phe346 shown as sticks. (**D**) Structural superposition of *Sso*–PCNA2 (olive) and the *E.coli* β-clamp protein (teal) (PDB code: 1UNN). The β-clamp was co-crystallized with the little finger domain of the DNA polymerase Pol IV (DinB), the interacting region of which is shown in stick representation.

PCNA orthologue IDCLs (Figure 6A). This also likely contributes to the observed client protein specificity between the *S.solfataricus* PCNA subunits.

Having elucidated the specificity of *Sso*–PCNA1 for the *Sso*–FEN1 client protein, *Sso*–PCNA2 was subsequently analysed for the basis of specificity for binding its client protein. DNA Polymerase B1 (*Sso*–Pol B1) has previously been shown to interact with *Sso*–PCNA2 through an N-terminal 9 residue PIP-box motif (13), which appears more closely related to the bacterial β-clamp-binding motif at the sequence level than to other clamp-binding motifs (Figure 6B) (26). The structural basis for recognition of this motif has been revealed by the structure of a complex between the little finger domain of the translesion DNA polymerase Pol IV/DinB of *E.coli* in complex with the β-clamp (29).

Superposition of the β-clamp from this complex (PDB code: 1UNN) onto *Sso*–PCNA2 reveals similarities between elements of the IDCL linker conformation and between the residues involved in the proposed interaction (see Figure 6D). In the *Ec*-Pol IV-β-clamp structure Gln346 of the *Ec*-Pol IV consensus sequence binds the β-clamp in a pocket between the side-chains of His175, Asn320, Tyr323 and Met364, and a similar pocket also exists in the *Sso*–PCNA2 structure for binding of Gln4 of *Sso*–PolB1. Finally, the hydrophobic anchor in the C-terminus of the *Ec*-Pol IV β-clamp-binding motif is provided by the tripeptide sequence Leu-Gly-Leu (29). In *Sso*–PolB1 the Leu7-Phe8 dipeptide is in the equivalent position and could bind in an analogous manner (26).

The classical PIP-box structure forms a 3_{10} helix formed by residues between the conserved glutamine and the double aromatic motif. However, the structure of the bacterial β-clamp-binding consensus motif does not have a helical segment, presumably because of fewer residues between the

conserved glutamine and the hydrophobic anchor. Though the double proline motif of the *Sso*–PCNA2 IDCL sterically precludes *Sso*–FEN1 PIP-box motif binding, it could however accommodate a peptide with the same conformation of *Ec*-Pol IV. This is demonstrated in the superposition of *Ec*-Pol IV peptide onto the *Sso*–PCNA2 structure (Figure 6D). Thus, the rigid double Proline motif present in the IDCL of *Sso*–PCNA2 plays a dual role in client protein specificity by sterically precluding *Sso*–FEN1 binding and also forming one side of the proposed *Sso*–PolB1 Leu7-Phe8 hydrophobic pocket.

The basis of client enzyme–PCNA interaction specificity in the *Sufolobus* system appears to reside in the sequence and structure of the PCNA subunit IDCL, in residues of PCNA in close proximity to the IDCL and in the client protein PIP-box sequence and structure. As with the inter-subunit interactions, the client interactions in the archaeal *Sulfolobus* system appear to combine elements of both the eukaryotic and bacterial PCNA systems.

FEN1 orientation by *Sso*–PCNA1

Studies of enzyme recruitment to eukaryotic PCNA rings are complicated by the ability of the homotrimeric clamp to bind multiple copies of the client. In the crystal structure of the human PCNA–FEN1 complex, each of the three FEN1 molecules bound to the PCNA ring adopts a different orientation with respect to its cognate PCNA subunit (Figure 7A–C) (12), making it very difficult to assign biological significance to any of those conformations. An important advantage of the heterotrimeric *S.solfataricus* PCNA system and its subunit specificity for client enzymes therefore, is the ability to

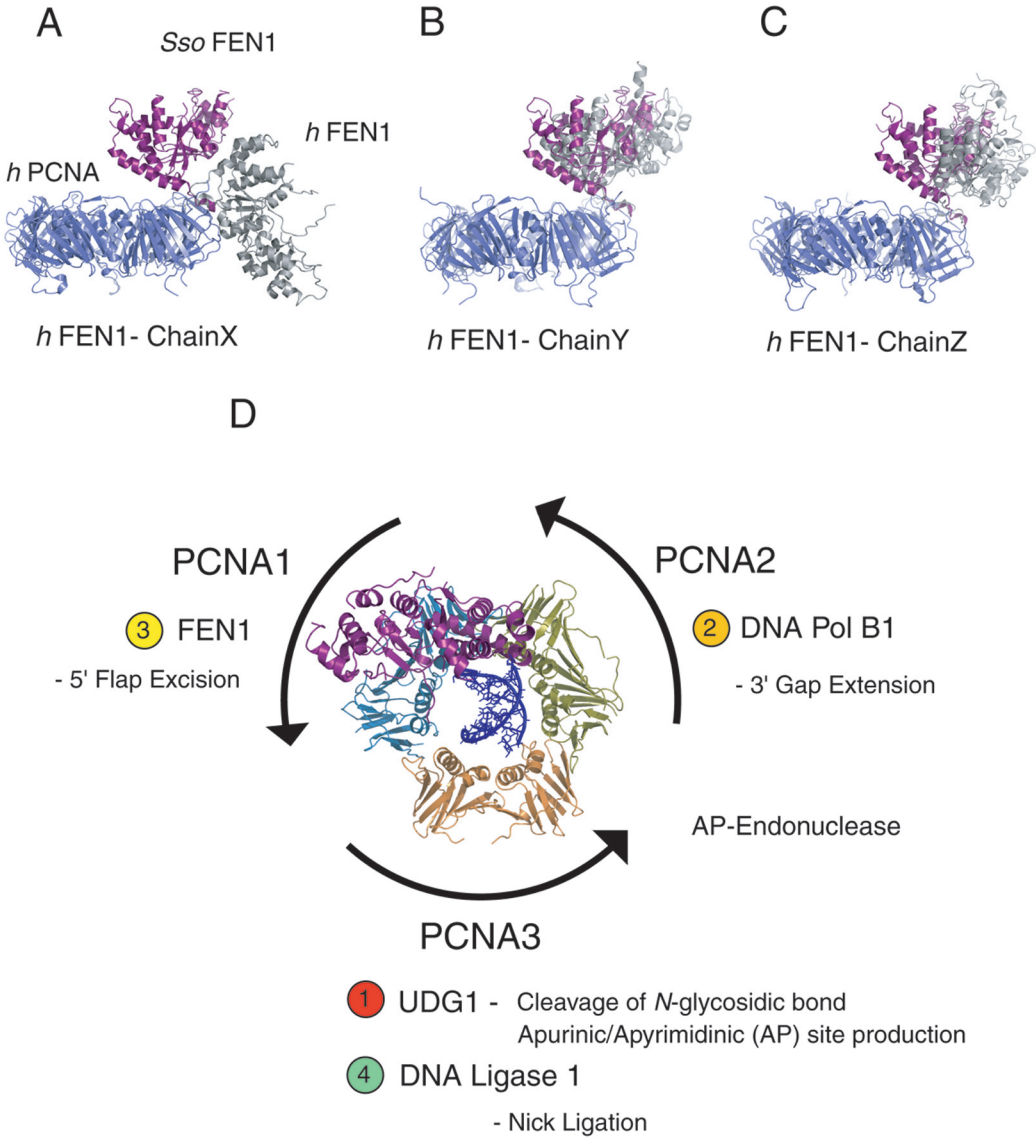

Figure 7. (**A–C**) Superposition of the *Sso*–PCNA1–FEN1 structure onto chains (**A**–C) of the human homotrimer suggests a physiologically relevant orientation of human FEN1 on the human PCNA assembly—(B) (pdb code : 1UL1, chain Y). The human PCNA homotrimer, human FEN1 and superposed *Sso*–FEN1 are coloured blue, grey and purple, respectively. (**D**) Model of DNA-binding to *Sso*–FEN1 based on superposition with the DNA bound *Afu*-FEN1 structure. The black arrows represent the direction of the hand-off of DNA intermediates around the PCNA ring in the sequential repair enzyme cascade mechanism.

trap, in essence, the correct stoichiometric complex in which the orientation and conformation of the client enzyme on the PCNA ring is far more likely to be functionally relevant.

When the *Sso*–PCNA1 component is used to superimpose the *Sso*–PCNA1–FEN1 complex in turn onto the three human PCNA subunits in the human PCNA–FEN1 structure, one of the three human FEN1 molecules (chain Y) is found to have a very similar orientation with respect to its PCNA subunit. Furthermore, the polypeptide chains containing the PIP-box motif in both *Sso*–FEN1 and human FEN1 chain Y have extremely similar conformations. In both cases, the enzyme makes additional interactions involving residues outside its PIP-box motif, with residues in the β-3–β-4 intervening loop of the associated PCNA subunit, which in combination with the PIP-box conformation, maintains this orientation of the FEN1 core with respect to the PCNA ring.

That the same FEN1–PCNA interaction and orientation is seen in proteins from two highly diverged species, and in the presence of very different crystal environments, suggests strongly that this is a biologically significant conformation. To gain further insight into this, we superimposed the FEN1 component of the *Afu*-FEN1–DNA complex onto the PCNA-bound *Sso*–FEN1, to model a fully assembled DNA bound *Sso*–FEN1–PCNA1–PCNA2–PCNA3 complex (Figure 7B). Superposition of residues involved in the 3′ flap substrate recognition results in a r.m.s.d. of 1.12 Å across 58 equivalent Cα positions in respect to *A.fulgidus* DNA bound FEN1. The low r.m.s.d. across this region demonstrates the conservation of the 3′-flap binding mode in the archaeal class of FEN1 enzymes. As can be seen, the double-stranded portion of the 3′-flap DNA substrate bound to FEN1 is positioned such that it could pass through the lumen of the *Sso*–PCNA ring, suggesting that we have crystallized a physiologically relevant orientation of FEN1 on PCNA, in which it is positioned for productive interaction with a DNA substrate encircled by the PCNA ring. We note however, that the helical axis of the double-stranded segment of the FEN1-bound DNA is not perpendicular to the PCNA ring, but is tilted by ∼30°. Although this complex is a model and changes in the conformation of the DNA and adaptor proteins may occur, it does suggest that the common assumption of DNA passing perpendicularly through toroidal clamps, without direct contact, may not be the case, especially when the DNA is engaged by a PCNA client enzyme.

PCNA coordination and orientation of enzyme cascades

The specificity of the *Sso*–PCNA heterotrimer subunits for their respective client proteins as demonstrated in this study, and previously (13), permits assignment of the chirality of the sequential enzyme cascade in the base excision repair and replication pathways as previously postulated (see Figure 7D) (11,27). Sequential action of a DNA polymerase, a 5′-flap endonuclease and a DNA ligase can achieve error-free 'long-patch' repair of a single-strand DNA gap generated by, e.g. base excision by a glycosylase and AP-endonuclease (7).

A uracil-DNA glycosylase (*Sso*-UDG1) has recently been characterized in *S.solfataricus* and shown to interact with *Sso*–PCNA3 (15). The arrival of a DNA glycosylase at the site of a lesion is the initiating step in the base excision repair pathway (32). After cleavage of the *N*-glycosidic bond, the AP site is removed by an AP-endonuclease, and the resulting single-strand gapped DNA passed to *Sso*-DNA polymerase B1, which is specific for binding to *Sso*–PCNA2 and performs displacement synthesis across the gap. Next, *Sso*–FEN1-bound to *Sso*–PCNA1, loads from the 5′ end of the flap and tracks back to the 5′-flap—duplex DNA junction (33). After removal of the flap, *Sso*-DNA ligase bound to *Sso*–PCNA3 completes the repair process through ligation of the nick (Figure 7D). It is of particular interest that the client enzymes for the first (UDG) and final (DNA ligase) step of the pathway bind the same PCNA subunit, thereby allowing time for client enzyme exchange on the PCNA ring during the intermediary steps of the repair pathway cascade. Thus, as the heterotrimeric PCNA rotates around the double helix, and translates back and forth along it, DNA repair and replication intermediates can be passed to the next client repair enzyme in a highly co-ordinated and regulated manner.

S.solfataricus has evolved three different PCNA subunits to control the correct assembly of client enzymes on the PCNA ring, and help select meaningful combinations from the plethora of possibilities. Eukaryotes also possess a hetrotrimeric system in addition to homotrimeric PCNA, formed by the Rad9, Rad1 and Hus1 proteins (34,35). While this so-called 9-1-1 complex is involved in specialized DNA damage signalling roles, including facilitation of the ATR-dependent phosphorylation and activation of Chk1 (36), it also appears to recapitulate many of the DNA repair enzyme recruitment activities of PCNA (37). However, unlike the *Sulfolobus* heterotrimeric PCNA, the individual subunits of 9-1-1 do not seem to have discriminatory binding sites, so that MYH, DNA Lig1, FEN1 and Polβ all appear to bind equally well to all three subunits (38–42). Despite the lack of an enzyme-selective clamp, as in *Sulfolobus*, higher eukaryotes are nonetheless presented with the same problem and have likely evolved an alternative mechanism for coordinating pathway assembly, although the nature of this is not yet clear. One possibility is that meaningful combinations are selected by specific lateral contacts between client enzymes attached to adjacent subunits, however further work will be required to test this hypothesis.

ACKNOWLEDGEMENTS

The authors would like to thank Dr David Komander for help with data collection, and Dr Maruf Ali for helpful discussions. This work was supported by Cancer Research UK (L.H.P.), S.D.B. is funded by the Medical Research Council, and would like to thank Isabelle Dionne for technical assistance. Atomic co-ordinates and structure factor amplitudes have been submitted to the RCS PDB with the accession code: 2izo. Funding to pay the Open Access publication charges for this article was provided by CR-UK (Cancer Research UK).

Conflict of interest statement. None declared.

REFERENCES

1. Hingorani,M.M. and O'Donnell,M. (2000) Sliding clamps: a (tail)ored fit. *Curr. Biol.*, **10**, R25–R29.

2. Kelman,Z. and O'Donnell,M. (1995) DNA polymerase III holoenzyme: structure and function of a chromosomal replicating machine. *Annu. Rev. Biochem.*, **64**, 171–200.
3. Gulbis,J.M., Kelman,Z., Hurwitz,J., O'Donnell,M. and Kuriyan,J. (1996) Structure of the C-terminal region of p21(WAF1/CIP1) complexed with human PCNA. *Cell*, **87**, 297–306.
4. Parker,A., Gu,Y., Mahoney,W., Lee,S.H., Singh,K.K. and Lu,A.L. (2001) Human homolog of the MutY repair protein (hMYH) physically interacts with proteins involved in long patch DNA base excision repair. *J. Biol. Chem.*, **276**, 5547–5555.
5. Oyama,M., Wakasugi,M., Hama,T., Hashidume,H., Iwakami,Y., Imai,R., Hoshino,S., Morioka,H., Ishigaki,Y., Nikaido,O. *et al.* (2004) Human NTH1 physically interacts with p53 and proliferating cell nuclear antigen. *Biochem. Biophys. Res. Commun.*, **321**, 183–191.
6. Krokan,H.E., Otterlei,M., Nilsen,H., Kavli,B., Skorpen,F., Andersen,S., Skjelbred,C., Akbari,M., Aas,P.A. and Slupphaug,G. (2001) Properties and functions of human uracil-DNA glycosylase from the UNG gene. *Prog. Nucleic Acid Res. Mol. Biol.*, **68**, 365–386.
7. Matsumoto,Y. (2001) Molecular mechanism of PCNA-dependent base excision repair. *Prog. Nucleic Acid Res. Mol. Biol.*, **68**, 129–138.
8. Dianova,I.I., Bohr,V.A. and Dianov,G.L. (2001) Interaction of human AP endonuclease 1 with flap endonuclease 1 and proliferating cell nuclear antigen involved in long-patch base excision repair. *Biochemistry*, **40**, 12639–12644.
9. Tsuchimoto,D., Sakai,Y., Sakumi,K., Nishioka,K., Sasaki,M., Fujiwara,T. and Nakabeppu,Y. (2001) Human APE2 protein is mostly localized in the nuclei and to some extent in the mitochondria, while nuclear APE2 is partly associated with proliferating cell nuclear antigen. *Nucleic Acids Res.*, **29**, 2349–2360.
10. Tom,S., Henricksen,L.A., Park,M.S. and Bambara,R.A. (2001) DNA ligase I and proliferating cell nuclear antigen form a functional complex. *J. Biol. Chem.*, **276**, 24817–24825.
11. Chapados,B.R., Hosfield,D.J., Han,S., Qiu,J., Yelent,B., Shen,B. and Tainer,J.A. (2004) Structural basis for FEN-1 substrate specificity and PCNA-mediated activation in DNA replication and repair. *Cell*, **116**, 39–50.
12. Sakurai,S., Kitano,K., Yamaguchi,H., Hamada,K., Okada,K., Fukuda,K., Uchida,M., Ohtsuka,E., Morioka,H. and Hakoshima,T. (2005) Structural basis for recruitment of human flap endonuclease 1 to PCNA. *EMBO J.*, **24**, 683–693.
13. Dionne,I., Nookala,R.K., Jackson,S.P., Doherty,A.J. and Bell,S.D. (2003) A heterotrimeric PCNA in the hyperthermophilic archaeon *Sulfolobus solfataricus*. *Mol. Cell*, **11**, 275–282.
14. Roberts,J.A., Bell,S.D. and White,M.F. (2003) An archaeal XPF repair endonuclease dependent on a heterotrimeric PCNA. *Mol. Microbiol.*, **48**, 361–371.
15. Dionne,I. and Bell,S.D. (2005) Characterization of an archaeal family 4 uracil DNA glycosylase and its interaction with PCNA and chromatin proteins. *Biochem. J.*, **387**, 859–863.
16. Leslie,A.G.W. (1992) Recent changes to the MOSFLM package for processing film and image plate data. *Joint CCP4 + ESF-EAMCB Newsletter on Protein Crystallography*, No. 26.
17. CCP4 (1994) Collaborative Computational Project Number 4. The CCP4 suite: programs fo protein crystallography. *Acta Crystallogr.*, **D50**, 760–763.
18. Storoni,L.C., McCoy,A.J. and Read,R.J. (2004) Likelihood-enhanced fast rotation functions. *Acta Cryst.*, **D60**, 432–438.
19. Hosfield,D.J., Mol,C.D., Shen,B. and Tainer,J.A. (1998) Structure of the DNA repair and replication endonuclease and exonuclease FEN-1: coupling DNA and PCNA binding to FEN-1 activity. *Cell*, **95**, 135–146.
20. Kontopidis,G., Wu,S.Y., Zheleva,D.I., Taylor,P., McInnes,C., Lane,D.P., Fischer,P.M. and Walkinshaw,M.D. (2005) Structural and biochemical studies of human proliferating cell nuclear antigen complexes provide a rationale for cyclin association and inhibitor design. *Proc. Natl Acad. Sci. USA*, **102**, 1871–1876.
21. Emsley,P. and Cowtan,K. (2004) Coot: model-building tools for molecular graphics. *Acta Crystallographica. Section D. Biol. Crystallography*, **60**, 2126–2132.
22. Brunger,A.T., Adams,P.D., Clore,G.M., DeLano,W.L., Gros,P., Grosse-Kuntsleve,R.W., Jiang,J.-S., Kuszewski,J., Nilges,M., Pannu,N.S. *et al.* (1998) Crystallography & NMR System: a new software suite for macromolecular structure determination. *Acta. Crystallographica. Section D. Biol. Crystallography*, **54**, 905–921.
23. Murshudov,G.N., Vagin,A.A. and Dodson,E.J. (1997) Refinement of macromolecular structures by the maximum-likelihood method. *Acta. Crystallographica. Section D. Biol. Crystallography*, **53**, 240–255.
24. DeLano,W.L. (2002) *The PyMOL User's Manual*. DeKano Scientific, San Carlos, CA, USA.
25. Shen,B., Nolan,J.P., Sklar,L.A. and Park,M.S. (1997) Functional analysis of point mutations in human flap endonuclease-1 active site. *Nucleic Acids Res.*, **25**, 3332–3338.
26. Dalrymple,B.P., Kongsuwan,K., Wijffels,G., Dixon,N.E. and Jennings,P.A. (2001) A universal protein–protein interaction motif in the eubacterial DNA replication and repair systems. *Proc. Natl Acad. Sci. USA*, **98**, 11627–11632.
27. Shamoo,Y. and Steitz,T.A. (1999) Building a replisome from interacting pieces: sliding clamp complexed to a peptide from DNA polymerase and a polymerase editing complex. *Cell*, **99**, 155–166.
28. Matsumiya,S., Ishino,S., Ishino,Y. and Morikawa,K. (2002) Physical interaction between proliferating cell nuclear antigen and replication factor C from *Pyrococcus furiosus*. *Genes Cells*, **7**, 911–922.
29. Bunting,K.A., Roe,S.M. and Pearl,L.H. (2003) Structural basis for recruitment of translesion DNA polymerase Pol IV/DinB to the beta-clamp. *EMBO J.*, **22**, 5883–5892.
30. Kong,X.P., Onrust,R., O'Donnell,M. and Kuriyan,J. (1992) Three-dimensional structure of the beta subunit of *E. coli*. DNA polymerase III holoenzyme: a sliding DNA clamp. *Cell*, **69**, 425–437.
31. Krishna,T.S., Kong,X.P., Gary,S., Burgers,P.M. and Kuriyan,J. (1994) Crystal structure of the eukaryotic DNA polymerase processivity factor PCNA. *Cell*, **79**, 1233–1243.
32. Pearl,L.H. (2000) Structure and function in the uracil-DNA glycosylase superfamily. *Mutat. Res.*, **460**, 165–181.
33. Murante,R.S., Rust,L. and Bambara,R.A. (1995) Calf 5′ to 3′ exo/endonuclease must slide from a 5′ end of the substrate to perform structure-specific cleavage. *J. Biol. Chem.*, **270**, 30377–30383.
34. Volkmer,E. and Karnitz,L.M. (1999) Human homologs of *Schizosaccharomyces pombe* rad1, hus1 and rad9 form a DNA damage-responsive protein complex. *J. Biol. Chem.*, **274**, 567–570.
35. Venclovas,C. and Thelen,M.P. (2000) Structure-based predictions of Rad1, Rad9, Hus1 and Rad17 participation in sliding clamp and clamp-loading complexes. *Nucleic Acids Res.*, **28**, 2481–2493.
36. Parrilla-Castellar,E.R., Arlander,S.J. and Karnitz,L. (2004) Dial 9-1-1 for DNA damage: the Rad9-Hus1-Rad1 (9-1-1) clamp complex. *DNA Repair (Amst)*, **3**, 1009–1014.
37. Helt,C.E., Wang,W., Keng,P.C. and Bambara,R.A. (2005) Evidence that DNA damage detection machinery participates in DNA repair. *Cell Cycle*, **4**, 529–532.
38. Smirnova,E., Toueille,M., Markkanen,E. and Hubscher,U. (2005) The human checkpoint sensor and alternative DNA clamp Rad9-Rad1-Hus1 modulates the activity of DNA ligase I, a component of the long-patch base excision repair machinery. *Biochem. J.*, **389**, 13–17.
39. Friedrich-Heineken,E., Toueille,M., Tannler,B., Burki,C., Ferrari,E., Hottiger,M.O. and Hubscher,U. (2005) The two DNA clamps Rad9/Rad1/Hus1 complex and proliferating cell nuclear antigen differentially regulate flap endonuclease 1 activity. *J. Mol. Biol.*, **353**, 980–989.
40. Chang,D.Y. and Lu,A.L. (2005) Interaction of checkpoint proteins Hus1/Rad1/Rad9 with DNA base excision repair enzyme MutY homolog in fission yeast, *Schizosaccharomyces pombe*. *J. Biol. Chem.*, **280**, 408–417.
41. Wang,W., Brandt,P., Rossi,M.L., Lindsey-Boltz,L., Podust,V., Fanning,E., Sancar,A. and Bambara,R.A. (2004) The human Rad9-Rad1-Hus1 checkpoint complex stimulates flap endonuclease 1. *Proc. Natl Acad. Sci. USA*, **101**, 16762–16767.
42. Toueille,M., El-Andaloussi,N., Frouin,I., Freire,R., Funk,D., Shevelev,I., Friedrich-Heineken,E., Villani,G., Hottiger,M.O. and Hubscher,U. (2004) The human Rad9/Rad1/Hus1 damage sensor clamp interacts with DNA polymerase beta and increases its DNA substrate utilisation efficiency: implications for DNA repair. *Nucleic Acids Res.*, **32**, 3316–3324.